Elementary Steps of the Catalytic NO_x Reduction with NH_3: Cluster Studies on Reactant Adsorption at Vanadium Oxide Substrate

M. Gruber and K. Hermann

Inorg. Chem. Dept., Fritz-Haber-Institut der Max-Planck-Gesellschaft,
Faradayweg 4-6, 14195 Berlin, Germany

Subject classification: 68.43.-h, 68.47.Gh, 82.65.+r, 71.15.Mb, 68.43.Pq, 68.43.Bc, 68.43.Fg

ABSTRACT

Extended cluster models together with density-functional theory (DFT) are used to evaluate geometric, energetic, and electronic properties of different adsorbate species that can occur at a vanadium oxide surface where the selective catalytic reduction (SCR) of NO in the presence of ammonia proceeds. Here we focus on atomic hydrogen, nitrogen, and oxygen, as well as molecular NO and NH_x, x = 1, 4, adsorption at a model V_2O_5(010) surface. Binding sites, oxygen and vanadium, at both the perfect and reduced surface are considered where reduction is modeled by (sub-) surface oxygen vacancies. The reactants are found to bind overall more strongly at oxygen vacancy sites of the reduced surface where they stabilize in positions formerly occupied by the oxygen (substitutional adsorption) compared with weaker binding at the perfect surface. In particular, ammonia, which interacts only weakly with vanadium at the perfect surface, binds quite strongly near surface oxygen vacancies. In contrast, surface binding of the NH_4 adsorbate species differs only little between the perfect and the reduced surface which is explained by the dominantly electrostatic nature of the adsorbate interaction. The theoretical results are consistent with experimental findings and confirm the importance of surface reduction for the reactant adsorption forming elementary steps of the SCR process.

1. INTRODUCTION

Transition metal oxides are of considerable scientific interest and great technological importance in fields which are as diverse as superconductivity or gas sensing[1]. Here vanadium oxides have attracted much attention because of their extremely interesting structural, electronic, and magnetic behavior[2]. In addition, they are involved as essential components in numerous catalysts due to the mobility of their surface and bulk oxygen atoms exhibiting different reactivity at different crystal faces combined with the existence of Lewis acid sites[3]. Important catalytic reactions, where VO_x based catalysts are actually used or represent promising candidates, include the oxidation and dehydrogenation of hydrocarbons[4], the oxidation of sulfur dioxide[5], the ammoxidation reaction to produce acrylonitrile[6, 7], or the selective catalytic reduction (SCR) of NO_x[8, 9]. In a number of these reactions ammonia has been found to improve yields and/or to serve as an essential reaction partner. The latter applies, in particular, to the selective catalytic reduction (SCR) of NO_x in the presence of ammonia which is the basic focus of the present study.

The SCR of NO_x is operative in large stationary sources, such as fossil-fuel power plants, where NO_x species is removed from the exhaust gas to yield N_2 and H_2O. This process is facilitated by the presence of NH_3 which participates in the reduction according to

$$4\ NH_3 + 4\ NO + O_2 \rightarrow 4\ N_2 + 6\ H_2O \qquad (1)$$

or

$$4\ NH_3 + 2\ NO_2 + O_2 \rightarrow 3\ N_2 + 6\ H_2O \quad . \qquad (2)$$

Here TiO_2-supported V_2O_5-WO_3 and V_2O_5-MoO_3 catalysts are predominant in industrial applications and continue to be developed further[9-15]. Because of its technological importance the SCR process at V_2O_5 based catalysts was the subject of numerous scientific studies at various levels. Nevertheless, microscopic details, such as the nature of the active site at the catalyst surface, are still under debate and various reaction mechanisms have been proposed in the literature, cp. Ref.[9] and references therein. Amongst others, nitrosamide (NH_2NO) species has been suggested as a key intermediate in the SCR reaction[9]. This is supported by mass spectroscopic data that indicate the presence of NH_2NO during the reaction of NH_3 with NO on vanadium oxide catalysts[16]. Moreover, NH_2NO was identified as intermediate in most of the

theoretical studies of the SCR reaction at clean as well as at TiO_2 supported V_2O_5 surfaces[17-21]. Further, theoretical studies showed that the reaction of NO with NH_2 in gas phase proceeds via the NH_2NO intermediate[22, 23].

It is generally agreed[9] that under dilute reaction conditions (a) NO is the actual reactant, according to (1) and not NO_2, (b) N_2O is not an intermediate, (c) the reaction is a coupling reaction of NO and NH_3 producing N_2, and (d) the reaction is redox type where O_2 reoxidizes the surface sites reduced by other reactants. Further, it is believed[9] that the redox reaction proceed according to a Mars-van-Krevelen mechanism[24] where the catalyst is chemically reduced by the formation of oxygen vacancies. Isotopic labeling studies claimed that such vacancies can be generated by desorption of water formed with surface oxygen[25, 26] where the required hydrogen is provided by the dehydrogenation of NH_3 during the reaction, see equation (1). In addition, ammonia adsorption is considered to be the initial reaction step while NO is believed to react from gas phase or from a weakly adsorbed state. Experiments show that NH_3 is adsorbed near OH groups at the oxide surface, which act as Brønsted acid sites and lead to surface NH_4^+ species, as well as near vanadium centers that provide Lewis acid sites[9]. Thus, both Lewis and Brønsted acid sites need to be considered in the SCR process. In contrast, theoretical studies found that at the perfect $V_2O_5(010)$ surface only Brønsted acid sites will be active for NH_3 adsorption and subsequent reaction with NO[18-20, 27].

Based on the experimental evidence and on details of previous theoretical studies, the SCR process of NO_x in the presence of NH_3 can be divided into three main elementary steps

(i) The initial interaction and adsorption of gas phase NH_3 and NO at the catalyst surface. Here relative surface binding energies of the adsorbate species have important implications for possible reaction mechanisms.

(ii) Dehydrogenation and hydrogenation of NH_x surface species, surface water and oxygen vacancy formation which contribute to the reaction. These processes are accompanied by adsorbate as well as surface oxygen diffusion.

(iii) Interaction of the different adsorbates with the NO near the surface involving bond breaking / making. Here possible reaction scenarios can be already assessed based on the findings in (i), (ii).

In the present theoretical study we focus on details of the elementary reaction step (i), i.e. adsorbate binding of the different species at the vanadium oxide surface. This includes ammonia, nitrogen, hydrogen, NO, as well as NH_x species, x = 1, 2, 4 produced by ammonia (de)hydrogenation processes at the surface. Here electronic, geometric, and energetic parameters are evaluated using reasonably large cluster models together with density-functional theory (DFT). Going beyond previous theoretical studies[18-20, 27-35] where only sections of the perfect V_2O_5 surface have been examined, we consider also models for sections of the reduced surface. The latter are simulated by local environments near surface oxygen vacancies which are assumed to being created during the SCR reaction[9]. Vanadium atoms near these vacancies become electronically reduced and are found to be much more reactive than those at the perfect surface. Thus, they are relevant for the SCR process. The experimental identification of NH_3 and NH_4 species at the vanadium oxide surface is possible with infrared (IR) spectroscopy probing characteristic vibrational properties of the adsorbates. Therefore, we have evaluated corresponding vibrational modes of these adsorbates at the perfect and reduced V_2O_5(010) surface to be compared with experiment. Surface diffusion of the adsorbates during the SCR process as well as specific reaction paths, elementary steps (ii), (iii), have also been studied in detail[36] and will be published separately.

In Section 2 we introduce the surface models and computational methods used in this work while Section 3 presents our results and discussion. Finally, Section 4 summarizes our conclusions.

2. THEORETICAL DETAILS

2.1 Geometry and Cluster Models

In the present work local surface regions of vanadia catalysts are modeled by those of the (010) surface of vanadium pentoxide, V_2O_5. Corresponding single crystals are characterized by a layer type orthorhombic lattice with lattice constants a = 11.519 Å, b = 4.373 Å, c= 3.564 Å[37-39]. The physical crystal layers, shown in Fig. 1, are composed of six planar atom layers (4 oxygen layers, 2 vanadium layers) and extend parallel to the (010) netplane following the nomenclature used e.g. in[37]. (For an alternative choice of the orthorhombic crystal axes, the layer netplane orientation may also be denoted by (001) as proposed in Ref.[39].)

There are three structurally different oxygen centers in each physical layer, terminal (vanadyl) oxygen, O(1), coordinated to one vanadium atom by a short bond ($d_{V\text{-}O}$ = 1.59 Å) and bridging oxygen, O(2) / O(3), coordinated to two or three vanadium atoms with V-O distances ranging between 1.78 Å and 2.02 Å. In the topmost layer at the V_2O_5(010) surface each of these differently coordinated oxygen species can point either inside the crystal or stick out of the surface with respect to the closest vanadium atom. This results in six different types of oxygen where, in the following, we denote oxygen pointing out of the surface by O(1), O(2), or O(3) while oxygen pointing into the bulk will be denoted by O(1'), O(2'), or O(3'), as shown in Fig. 1.

Previous theoretical studies have shown that the electronic interaction between adjacent physical layers in bulk V_2O_5 along (010) is rather weak[40-42]. Therefore, we model local sections at the perfect V_2O_5(010) surface by reasonably large clusters cut out from one or two physical layers where vanadium and oxygen positions are taken from the experimental bulk structure. In order to simulate the electronic coupling of the local clusters with their atom environment of the V_2O_5 bulk (embedding) dangling bonds of peripheral oxygen atoms, arising from broken O-V bonds, are saturated by hydrogen positioned along the virtual O-V bond direction at a distance of 0.99 Å from the oxygen. This procedure has proven to be rather successful in a number of different cluster studies on vanadium pentoxide as well as other transition metal oxide substrates, such as V_2O_3 or MoO_3[2]. In this work we consider, amongst others, surface clusters $V_{10}O_{31}H_{12}$,

$V_{14}O_{46}H_{22}$, and $V_{14}O_{42}H_{14}$ (single layer models, Figs. 2a, b, c), and $V_{12}O_{40}H_{20}$, $V_{12}O_{40}H_{20}{}^{*}$ (double layer models, Figs. 2d, e). Here the single layer clusters $V_{10}O_{31}H_{12}$ and $V_{14}O_{46}H_{22}$, can be used to simulate the local environments near O(1), O($2^{(')}$), and O($3^{(')}$) oxygen as well as near vanadium sites at the V_2O_5(010) surface. Cluster $V_{14}O_{42}H_{14}$ is used to describe adsorption sites above the O(1) ridge and between O($2^{(')}$) sites. Further, the two double layer clusters $V_{12}O_{40}H_{20}$ and $V_{12}O_{40}H_{20}{}^{*}$, consisting of a top layer $V_{10}O_{31}H_{12}$ and a second layer $V_2O_9H_8$ part, allow a reasonable treatment of inter-layer coupling which becomes relevant for sub-surface O(1') sites.

Apart from cluster models simulating local sites at the perfect V_2O_5(010) surface we consider also models of the reduced surface. Here reduction is represented by local clusters with missing oxygen atoms. Since the V_2O_5(010) surface contains six structurally different types of oxygen it allows for six different oxygen vacancies O($1^{(')}$)$_{vac}$, O($2^{(')}$)$_{vac}$, and O($3^{(')}$)$_{vac}$. Local environments of these vacancies can be described by clusters $V_{10}O_{31}H_{12}$, $V_{14}O_{46}H_{22}$ of Figs. 2a, b (for vacancies O($2^{(')}$)$_{vac}$,O($3^{(')}$)$_{vac}$), $V_{12}O_{40}H_{20}$ of Figs. 2c, d (for vacancy O(1)$_{vac}$), and $V_{12}O_{40}H_{20}{}^{*}$ of Fig. 2e (for vacancy O(1')$_{vac}$) where in each clusters the oxygen atom is removed from the corresponding site. Note that, as a result of the crystal symmetry, the double layer clusters $V_{12}O_{40}H_{20}{}^{*}$ and $V_{12}O_{40}H_{20}$ consist of the same top layer $V_{10}O_{31}H_{12}$ and second layer $V_2O_9H_8$ parts but differ by the two component layers of $V_{12}O_{40}H_{20}$ being turned upside down in $V_{12}O_{40}H_{20}{}^{*}$.

All surface clusters reflecting initially the geometry of the ideal V_2O_5 crystal are allowed to relax locally in geometry optimizations. Here, depending on the oxygen or oxygen vacancy site, selected neighboring oxygen and vanadium atoms (nearest and next nearest neighbors) are included while the positions of all other cluster atoms are kept fixed.

2.2 Electronic Structure and Energetics

The electronic structure of the clusters described above are evaluated within density-functional theory (DFT) using the cluster code StoBe[43] where the gradient corrected revised Perdew-Burke-Ernzerhof (RPBE) exchange-correlation functional[44-46], as modified by Hammer

et al.[47], is employed, see below. Corresponding Kohn-Sham orbitals are represented by linear combinations of atomic orbitals (LCAOs) using basis sets of contracted Gaussians. The basis sets are of double zeta valence plus polarization (DZVP) quality, (63321/531/41) for vanadium, (7111/411/1) for oxygen and nitrogen, and (3111/111) for hydrogen[43]. Further, saturator hydrogen at the cluster periphery is represented by lower quality (311/1) contractions which was found to be sufficient in test calculations. Cluster ground states with spin multiplicity other than singlet are obtained by spin polarized calculations. Atom charges of the clusters in their ground states are evaluated by Bader charge analyses[48] and will be referred to as atom charges *q* in the following.

The adsorption and binding of atoms and small molecules at the perfect and reduced vanadium oxide surface is modeled in total energy minimizations based on geometry optimizations. In these calculations the corresponding adsorbates A (A = H, N, NO, NH_x) are placed near different oxygen and vanadium surface sites of the substrate clusters $V_aO_bH_c$ and geometry optimized according to lowest total energy of the compound cluster $V_aO_bH_c$+A. Then the adsorption energy is defined in a first step by

$$E_{ads}^{f}(A) = E_{tot}^{r}(V_aO_bH_c + A) - E_{tot}^{f}(V_aO_bH_c) - E_{tot}(A) \qquad (3)$$

where $E_{tot}^{r}(V_aO_bH_c + A)$ is the total energy of the compound cluster at the equilibrium geometry while $E_{tot}^{f}(V_aO_bH_c)$ and $E_{tot}(A)$ are total energies of the substrate cluster with all atoms fixed at their ideal bulk positions and of the adsorbate A, respectively. As mentioned earlier, the geometry optimization of the compound cluster includes substrate atoms near the adsorption site. These atoms may already deviate slightly from their ideal bulk positions in the equilibrated substrate cluster $V_aO_bH_c$ as a result of the local cluster approach. This artifact is corrected in a second step by evaluating equilibrium positions of the corresponding atoms in the substrate cluster leading to a relaxed total energy $E_{tot}^{r}(V_aO_bH_c)$. Then the corrected adsorption energy $E_{ads}(A)$ is calculated as

$$\begin{aligned} E_{ads}(A) &= E_{ads}^{f}(A) + E_{tot}^{f}(V_aO_bH_c) - E_{tot}^{r}(V_aO_bH_c) = \\ &= E_{tot}^{r}(V_aO_bH_c + A) - E_{tot}^{r}(V_aO_bH_c) - E_{tot}(A) \end{aligned} \qquad (4)$$

Note than with this definition exothermic adsorption will always be characterized by negative adsorption energies E_{ads}(A). In the following, we will use definition (4) for all numerical evaluations of E_{ads}(A).

The present model studies are based exclusively on the use of the revised RPBE exchange-correlation functional[44-47] which has shown to yield rather reliable adsorption energies for oxygen and small molecules at metal surfaces[47]. Obviously, the choice of other gradient corrected functionals, apart from general deficiencies of DFT to describe weak interactions, will affect the numerical results[49, 50] and may even lead to somewhat different qualitative behavior of certain physical quantities. Examples are the appearance of localized electronic gap states in reduced V_2O_5 bulk and the amount of localization, which has been corrected empirically by fitting the U parameter to reproduce experimental data in GGA+U studies[50]. However, we expect that the general physical trends concerning adsorbate energetics and geometries at the V_2O_5(010) surface will not be affected by the choice of the functional and are correctly described by the present approach.

3. Results and Discussion

Experimental studies on the adsorption and reaction of small molecules, which are relevant for elementary steps of the selective catalytic reduction of NO_x at vanadium oxide surfaces, have focused mainly on ammonia[51-56]. Here experimental techniques such as temperature programmed desorption (TPD)[51], Fourier transform infrared spectroscopy (FTIR)[52-54] and combined TPD-FTIR[55, 56] have been applied. After adsorption of NH_3 at the V_2O_5(010) surface two different surface species have been discussed[9, 57, 58]. First, surface ammonium ions, NH_4^+ are believed to result from NH_3 adsorption at OH groups (Brønsted acid sites)[52-54]. Second, ammonia is assumed to adsorb near vanadium centers (Lewis acid sites)[52-54] The latter species is often denoted by "coordinated ammonia" and claimed to be more stable at the surface than NH_4^+ which is based on findings that, after heating the V_2O_5 sample, typical IR bands of NH_4^+ disappear while those of NH_3 adsorbate species remain[52, 54]. These results have been verified for both V_2O_5 bulk substrate and for thin V_2O_5 films on TiO_2 support[9]. Ammonia adsorption

energies were estimated to be in the range between -0.8 eV and -1.1 eV[55]. In a number of experimental studies on NH_3 adsorption at vanadium oxide surfaces additional spectroscopic features have been found which could indicate the presence of a surface amide, NH_2[54, 59, 60]. This species, in addition to coordinated ammonia and NH_4^+ at the surface, was also suggested by nuclear magnetic resonance (NMR) measurements[61]. In contrast to ammonia adsorption there are only few experimental studies on NO adsorption at vanadium oxide surfaces which indicate that NO interacts only weakly with surfaces of V_2O_5 bulk substrate and for thin V_2O_5 films[9].

In theoretical studies, adsorption properties have been evaluated for hydrogen[28-33], NO[20, 31], and NH_3[18-20, 27, 31, 34] at the perfect V_2O_5(010) surface using cluster[18-20, 27-31] as well as periodic[32-34] surface models. There is a general agreement that hydrogen can form bonds with all oxygen sites, O(1), O(2), and O(3), at the perfect V_2O_5(010) surface but not with vanadium sites. These findings and corresponding equilibrium geometries of adsorbed hydrogen have been confirmed in the present calculations and will be recapitulated briefly in Section 3.1. Further, theoretical studies conclude that NO does not stabilize at the V_2O_5(010) surface[20, 31]. Various investigations of NH_3 adsorption at the perfect V_2O_5(010) surface[18-20, 27, 31, 34] demonstrate, in accordance with experiments, that a very stable NH_4^+ species can be formed by ammonia adsorption at already existing surface OH groups acting as Brønsted acid sites. Here computed adsorption energies range between -0.5 eV and -1.4 eV. In these studies NH_3 was never found to bind strongly at vanadium sites of the perfect V_2O_5(010) surface acting as Lewis acid sites. Only two studies report weak NH_3 adsorption near vanadium sites at rather large distance V-NH_3 distances, d(V-NH_3) = 2.54 Å[31] and = 2. 28 Å[34], respectively, yielding quite small adsorption energies E_{ads}(NH_3) of order -0.3 eV. Thus, "coordinated ammonia" at the perfect V_2O_5(010), surface suggested by experiment[52-54], has not been confirmed by theoretical work so far.

3.1. Adsorption at the perfect V_2O_5(010) surface

In the following, we consider adsorption near the five different oxygen sites, O(1), O(2$^{(')}$), O(3$^{(')}$), as well as near the vanadium site V at the perfect V_2O_5(010) surface, see Fig. 1. Different adsorbates, which are relevant for the selective catalytic reduction of NO, i.e. H, N, NO, and

NH_x, (x = 1,…4), are placed near these surface sites and are geometry optimized, including local surface relaxation as discussed in Sec. 2. Table 1 lists adsorption energies, E_{ads}, evaluated according to eq. (4). Here missing entries refer to cases where no stable adsorption could be found for the corresponding site. Further, Table 2 collects typical adsorbate - substrate distances characterizing the calculated equilibrium geometries and Fig. 3 visualizes, for each adsorbate, the energetically most preferred equilibrium structure. Results from Tables 1, 2 will be discussed in the following.

3.1.1. H, N, NH, NH_2, and NO adsorption

Atomic hydrogen is found to adsorb near all oxygen sites of the V_2O_5(010) surface, forming stable OH groups with reasonably large H adsorption energies E_{ads}(H) where, according to Table 1, the bridging O(2) site is energetically somewhat more favorable than the others. However, the overall variation of E_{ads}(H) amounting to 0.4 eV is rather moderate. In all cases, corresponding O-H bond lengths d(O-H) amount to about 1 Å, see Table 2, which is characteristic for OH species inside molecules. In addition, hydrogen becomes positively charged inside the OH, as indicated by Bader charges of q(H) = 0.6 au, while the OH species itself becomes negative at the surface. This is to be expected and reflects, together with corresponding H and O orbital hybridization the mixed ionic and covalent character of typical O-H binding.

As a consequence of OH bond formation, the binding of the corresponding surface oxygen with its vanadium neighbors is weakened. This is reflected in increased inter-atomic V-O distances at the relaxed V_2O_5 surface near the adsorption sites with increases of 0.1 to 0.2 Å, see Table 2. The O(2') and O(3') sites are located between or near two vanadyl groups each, VO(1), that stick out of the surface, see Fig. 1. These vanadyl groups participate in the adsorption-induced surface relaxation by moving outside and tilting away from the corresponding O(2') and O(3') sites which increases the O(1)-O(1) distances of the neighboring vanadyl oxygen species by 1.2 Å and 0.9 Å, respectively. As a result, the surface opens to accommodate the hydrogen adsorbate above the surface oxygen which itself is pulled slightly outside. This is illustrated in

Fig. 4 for hydrogen adsorption at the O(2') site where white balls represent the geometric structure at the perfect V_2O_5(010) surface while shaded balls reflect the structure after adsorption with arrows denoting adsorption-induced atom shifts near the adsorption site.

Although the equilibrium structures near the O(2') and O(3') sites after H adsorption differ considerably from those of their O(2) and O(3) counterparts, corresponding V-O bond lengths are quite similar. This suggests a rather flexible V-O network where bond angles can change but inter-atomic distances are more or less fixed. It is consistent with the small differences between adsorption energies E_{ads}(H) at O(2) and O(2') sites (and at O(3) and O(3') sites) amounting to only 0.15 eV, see Table 1. Previous theoretical studies[28-33] did not consider O(2') and O(3') sites for hydrogen adsorption[29, 31-33] or reported significantly smaller adsorption energies for these sites[28, 30]. The strong hydrogen adsorption at O(2') and O(3') found in the present work can be understood as a consequence of allowing for improved substrate relaxation in the presence of the adsorbate by including more surface atoms compared with those considered previously[28, 30]. While the adsorption energies E_{ads}(H) for the O(2') and O(2) sites are similar, hydrogen adsorption is likely to favor the O(2) site. The adsorption path for O(2') passing (and tilting) the two vanadyl groups near O(2') may be energetically costly and possibly involves an adsorption barrier before the adsorbate can stabilize at the surface. Likewise, the O(3') and O(3) sites with similar E_{ads}(H) values will favor the O(3) site over O(3') for the same reason. Finally, the entry for E_{ads}(H) at a vanadium site of the V_2O_5(010) surface is missing in Table 1 which documents that hydrogen cannot stabilize at the bare metal site. In contrast, hydrogen is found to adsorb at all oxygen sites of the surface. This poses the question of the adsorbate diffusing between adjacent oxygen sites which may become important in connection with possible surface reactions involving hydrogen. This subject is discussed elsewhere in greater detail[36, 62].

Table 1 lists also adsorption energies E_{ads} for **atomic nitrogen** at the V_2O_5(010) surface. Here nitrogen is found to bind at all oxygen sites except O(3') forming stable surface NO species with, however, corresponding E_{ads} values depending strongly on the surface site. The vanadyl O(1) site is energetically by far the most preferred with an adsorption energy of E_{ads}(N) = -1.54 eV. At this site the N-O bond length of 1.21 Å, see Table 2, is the smallest of all sites and close to 1.15 Å observed for gas phase NO[63]. The adsorbed nitrogen becomes positively charged inside

the NO, as indicated by Bader charges of q(N) = 0.4 au, while the NO species itself is negative at the surface and its orbital structure resembles that of gas phase NO. Further, NO bond formation at the surface weakens the binding of the corresponding surface oxygen with its vanadium neighbors. This becomes obvious, as for hydrogen adsorption, by increased inter-atomic V-O distances near the adsorption sites where the increases amount to about 0.25 Å, see Table 2.

Adsorption of **NH and NH_2** species at the V_2O_5(010) surface leads to binding at all oxygen sites except O(2') and O(3'). In addition, NH_2 can stabilize above a bare vanadium site with, however, rather weak binding characterized by $E_{ads}(NH_2)$ = -0.12 eV. The E_{ads} values of Table 1 show that the energetically preferred adsorption sites are O(1) for NH and O(2) for NH_2, respectively, where both radicals stabilize in a tilted geometry as sketched in Fig. 3 and are positively charged (Bader charges near 0.3 au). The adsorption leads to adsorbate – substrate distances, represented by inter-atomic distances d(O-N), which increase from NH (d(O(1)-N) = 1.30 Å) to NH_2 (d(O(2)-N) = 1.45 Å) and are both larger than for nitrogen adsorption (d(O(1)-N) = 1.21 Å). This can be understood as gradually weaker chemisorptive binding at oxygen sites in going from nitrogen to NH to NH_2 adsorption which is obvious from Table 1 and expected on chemical grounds. Both NH and NH_2 do not stabilize at the bridging sites O(2') and O(3') which may be explained as a simple geometric effect (steric hindrance). Due to their size the two radicals cannot be accommodated between the vanadyl oxygen groups enclosing the oxygen sites O(2') and O(3') and no additional vanadyl - adsorbate bonds can be formed that may help to stabilize the adsorbates.

Nitric oxide, NO, is found to interact rather weakly with the perfect V_2O_5(010) surface where only sites above the vanadyl O(1) ridge and above bridging O(2) can serve as stable adsorption sites with quite small adsorption energies E_{ads}(NO) of -0.28 eV and -0.20 eV, respectively, see Table 1. Here the energetically favored adsorption is described geometrically by the NO positioned near the center of four adjacent O(1) sites at the vanadyl ridge of the V_2O_5(010) surface, shown in Fig. 3, with its molecular axis pointing almost parallel to the surface. As a result, corresponding inter-atomic distances d(O-N) are rather large, approximately 3 Å (cp. Table 2), which is consistent with weak adsorptive binding.

3.1.2. NH_3 and NH_4 adsorption

The calculations show for **ammonia**, NH_3, adsorption that the molecule interacts weakly with the perfect V_2O_5(010) surface where it can stabilize only on top of a bare vanadium site at a rather large distance, d(V-N) = 2.70 Å, see Fig. 3 and Table 2. The corresponding adsorption energy, E_{ads} = -0.25 eV, is quite small and the molecule retains its free molecule character accumulating only little positive charge, $q(NH_3)$ = 0.08 au. from Bader charges. This is in qualitatively good agreement with previous theoretical studies[18-22, 24, 35] but contrasts with results from experimental work which indicate that the NH_3 surface species binds at vanadium Lewis acid sites of the vanadium oxide surface[52-54]. The discrepancy may be explained by the existence of surface imperfections in the experiment where surface oxygen vacancies are good candidates as will be discussed below.

The **ammonium** species, NH_4, can equilibrate near vanadium and near all oxygen sites of the V_2O_5(010) surface, except for the O(2') site. The latter can be explained by steric repulsion due to the size of the molecule which does not fit between the two vanadyl groups surrounding the bridging O(2') site. In addition, the size of the tetrahedrally shaped NH_4 leads to equilibrium geometries which may involve more than one oxygen site at the surface. This happens for the energetically most favorable geometry where NH_4 binds with its nitrogen above the center of four O(1) vanadyl oxygen groups of the surface, as shown in Fig. 3, with a rather large adsorption energy, E_{ads} = -3.90 eV, see Table 1. Thus, the nitrogen of NH_4 does not couple directly with the oxygen groups forming covalent N-O bonds and reflected by corresponding orbital hybridization, as was found for the NH and NH_2 species. Instead, surface binding of the NH_4 species is mainly determined by electrostatic contributions as a consequence of the positive charge assumed by the NH_4 at the surface with values $q(NH_4)$ = 0.9 au. on average. This is in good agreement with results from previous theoretical studies[18-20, 27, 31, 34] and confirms the experimental observation that positively charged surface ammonium ions, NH_4^+, are produced by NH_3 adsorption[52-54]. The orbital analysis shows further that the hydrogen at the periphery of adsorbed NH_4 does not interact strongly with surface oxygen to form OH-type binding which is consistent with corresponding O-H distances yielding relatively large values, 1.8 Å, for the energetically preferred geometry of the NH_4 adsorbate.

The most stable position of the NH_4 adsorbate above four O(1) vanadyl oxygen groups of the V_2O_5(010) surface, see Fig. 3, agrees with that found by Yuan et al.[20]. In contrast, other theoretical studies[18, 19, 27, 31, 34] conclude that NH_4 stabilizes on top of the surface ridge formed by O(1) vanadyl oxygen groups with two of its hydrogen atoms pointing toward two adjacent O(1) centers and the other two sticking out of the surface. This geometry was identified in the present calculations, allowing for detailed surface relaxation, as a saddle point rather than an energy minimum. The discrepancy may be explained by the fact that the underlying potential energy surface (PES) is very flat and energy differences are rather small. On the other hand, some of the studies[19, 27] consider only very small model clusters with two vanadium centers, $V_2O_xH_y$, which cannot account for the equilibrium geometry found in the present study.

The rather large binding energy of NH_4 with the V_2O_5(010) surface, $E_{ads}(NH_4)$ = -3.90 eV, corresponds to a fictitious adsorption of a neutral gas phase NH_4 species. This cannot be considered realistic in view of an elementary step happening in a catalytic surface reaction since the NH_4 species will not exist in gas phase. However, the NH_4 surface species is likely to be produced as a result of hydrogenation of adsorbed NH_3 at the surface or by adsorption of gas phase NH_3 at surface OH groups (Brønsted acid sites) resulting from previous surface reactions. In the latter case, the binding energy of NH_3 at an OH site can be evaluated from cluster total energies according to

$$E_{ads}(OH/NH_3) = E_{tot}^{r}(S+NH_4) - E_{tot}(NH_3) - E_{tot}^{r}(S+H). \quad (5)$$

where $S+NH_4$ denotes the substrate cluster with adsorbed ammonium and S+H that with adsorbed hydrogen. Computed energies $E_{ads}(OH/NH_3)$ are listed in Table 1 and range between -0.88 eV for OH at the O(2) site and -1.40 eV for OH at the O(1) site. This shows that ammonia adsorption at Brønsted acid sites of the V_2O_5(010) surface can lead to fairly strong surface binding in contrast to quite weak NH_3 adsorption at the perfect surface without OH groups. Thus, pre-adsorbed surface OH groups can favor ammonia adsorption. In addition, the numerical values for $E_{ads}(OH/NH_3)$ are quite reasonable in comparison with experimental estimates of adsorption energies between -0.8 and -1.1 eV[55].

3.2. Adsorption at the reduced V_2O_5(010) surface

In this work, local sections of the reduced V_2O_5(010) surface are modeled by clusters where, in addition, oxygen vacancies are introduced to change the electronic configuration at the surface. Electronic and geometric properties of oxygen vacancies at the perfect V_2O_5(010) surface were the subject of various theoretical studies[2, 28-30, 32, 36, 49, 50, 64-68]. Therefore, in this work numerical results for oxygen vacancies have been evaluated mainly for the purpose of consistency with the present model clusters used to obtain adsorption parameters. Here we consider, in addition to surface vacancies at the five different oxygen sites, O(1), O($2^{(')}$), O($3^{(')}$), also a possible vacancy at the sub-surface oxygen site O(1'), see Figs. 1, 2. The latter has not been discussed in the literature so far. Corresponding results will be reviewed very briefly in Sec. 3.2.1.

The adsorption at the reduced V_2O_5(010) surface is modeled by appropriate vacancy clusters where the adsorbates, which are relevant for the selective catalytic reduction of NO, i.e. H, N, NO, and NH_x, (x = 1,…4), are placed near the five different oxygen vacancy sites, $O(1)_{vac}$, $O(2^{(')})_{vac}$, and $O(3^{(')})_{vac}$, and are geometry optimized. For the sub-surface vacancy $O(1')_{vac}$, the optimization refers to placing the adsorbate on top of the vanadium site above the vacancy. Therefore, this geometry will be denoted as $V/O(1')_{vac}$ in the following. The optimizations include, for all sites, local surface relaxation due to the missing oxygen at the vacancy but also relaxation as a result of the presence of the adsorbate as discussed in Sec. 2. Table 3 lists corresponding adsorption energies, E_{ads}, evaluated according to eq. (4) where the substrate clusters $V_aO_bH_c$ include appropriate oxygen vacancies. Missing entries in Table 3 denote cases where no stable adsorption could be found for the corresponding vacancy site. Table 4 gives typical adsorbate - substrate distances reflecting the calculated equilibrium geometries and Fig. 5 visualizes, for each adsorbate, the energetically most preferred equilibrium structure. Results from Tables 3, 4 will be discussed further below.

3.2.1. Oxygen vacancies at the perfect V_2O_5(010) surface

The existence of oxygen vacancies at the perfect $V_2O_5(010)$ surface has been confirmed by experiment[69-73] where scanning tunneling microscopy (STM) and angle-resolved X-ray photoelectron spectroscopy (ARXPS) experiments suggest vacancies at vanadyl O(1) sites[69-71]. (In the following we denote a vacancy created by removing oxygen from an O(X) site of the surface by $O(X)_{vac}$.) In contrast, high resolution electron energy loss spectroscopy (HREELS) data indicates that $O(2)_{vac}$ vacancies are predominant[72] while angle-resolved ultraviolet photoelectron spectroscopy (ARUPS) hints at the presence of $O(2)_{vac}$ and/or $O(3)_{vac}$ vacancies[73].

Geometric as well as electronic properties of oxygen vacancies at different $V_2O_5(010)$ surface sites, $O(1^{(')})_{vac}$, $O(2^{(')})_{vac}$, $O(3^{(')})_{vac}$, have also been studied extensively by theory employing cluster[2, 28-30, 36, 49, 67, 68] as well as periodic[32, 50, 64-66] models. These studies show that after removal of an oxygen atom from the oxide surface the vanadium neighbors of the resulting vacancy bind more strongly with their oxygen partners remaining in the substrate. The effect is most obvious for the vanadyl oxygen vacancy $O(1)_{vac}$. Here the vanadium atom below the vacancy moves from its initial position at the perfect $V_2O_5(010)$ surface by 0.98 Å into the substrate (cp. Table 5) where it approaches a vanadyl oxygen O(1) of the second physical layer, see Fig. 1, and forms a V-O-V bond bridge between the first and second physical layer. This bond is quite similar to binding in the lateral V-O(2)-V bridge at the surface. In contrast, to $O(1)_{vac}$, vacancy-induced shifts of the substrate atoms are much less pronounced for the other oxygen vacancies, $O(2^{(')})_{vac}$, $O(3^{(')})_{vac}$, are mainly restricted to lateral movements along the surface layer.

Table 6 lists oxygen vacancy formation energies E_D evaluated from the present model clusters. Here $E_D(O)$ refers to free oxygen atoms as the desorption limit with $E_D(O)$ defined by total energy differences

$$E_D(O) = E_{tot}^{r}(S_{vac}) + E_{tot}(O) - E_{tot}^{r}(S) \quad (6)$$

where $E_{tot}^{r}(S_{vac})$ and $E_{tot}^{r}(S)$ denote total energies of the substrate clusters representing the (relaxed) $V_2O_5(010)$ surface with and without an oxygen vacancy and $E_{tot}(O)$ refers to a free oxygen atom. As an alternative, the desorption limit could also use molecular O_2 in gas phase as a reference which yields a vacancy formation energy per atom $E_D(½O_2)$ given by

$$E_D(½O_2) = E_D(O) + ½\, E_B(O_2) \quad (7)$$

where $E_B(O_2)$ is the dissociation energy of gas phase O_2, evaluated as -2.79 eV for the present oxygen basis set and functional. The numerical values of Table 6 show that oxygen vacancy formation at the O(1) site is energetically the most favorable. This is in agreement with previous theoretical studies[2, 28-30, 32, 36, 49, 50, 64-68]. Further, computed vacancy geometries confirm those of previous studies. Previous studies yield absolute formation energies which may differ somewhat from the present values. This can be explained by different choices of the local atom environment allowed to relax during the vacancy formation which yields different relaxation contributions to the formation energy. In addition, the use of different exchange and correlation functionals in the DFT treatment of the systems influences formation energies. As an illustration we mention DFT studies employing GGA-hybrid[49] and GGA + U functionals[50] which report oxygen vacancy formation energies that are smaller than the present values of Table 6 by up to 0.7 eV while the ordering of the energies agrees with that of the present calculations.

The numerical results for the vacancy formation energies at $O(2)_{vac}$ and $O(2')_{vac}$ sites are identical in Table 6 while they are expected to differ slightly at the real $V_2O_5(010)$ surface. This is explained by the fact that the model clusters used to evaluate these energies include sections of only one physical $V_2O_5(010)$ layer, see Figs. 2a,b, where the local environment of the $O(2)_{vac}$ and $O(2')_{vac}$ sites is geometrically equivalent by symmetry. The same holds for $O(3)_{vac}$ and $O(3')_{vac}$ sites which show identical energies in Table 6. The use of sections of single physical layers to model $O(2^{(')})$ and $O(3^{(')})$ vacancies is justified by the result that in these cases vacancy-induced geometric relaxation is determined mainly by lateral atom movements where the electronic coupling between adjacent layers is negligible.

In the V_2O_5 bulk the two vanadyl oxygen sites O(1) and O(1') are equivalent by symmetry. In contrast, at the $V_2O_5(010)$ surface they must differ with O(1) referring to the vanadyl group sticking out of the surface and O(1') denoting a sub-surface vanadyl species, see Fig. 1. Likewise the vacancies $O(1)_{vac}$ and $O(1')_{vac}$ must differ where the sub-surface vacancy $O(1')_{vac}$ has not been considered so far. However, the latter vacancy may result from oxygen diffusing from the V_2O_5 bulk, filling a surface oxygen vacancy, and will affect the vanadium atom above it which is exposed at the surface and becomes reduced. As a consequence, the vanadium moves slightly out of the surface (by about 0.2 Å) and becomes more reactive than at the perfect surface without a

$O(1')_{vac}$ vacancy. This can affect adsorption at corresponding vanadium surface sites $V/O(1')_{vac}$. Therefore, in this work we also examine structural and electronic properties of the sub-surface oxygen vacancy $O(1')_{vac}$. The removal of a sub-surface oxygen at O(1') causes the vanadium above the oxygen site to relax upwards while the vanadium forming a V-O(2)-V bridge with the former shifts downwards. In addition, the corresponding O(2) atom moves downwards by 0.52 Å to form an almost linear V-O(2)-V bridge, as illustrated in Fig. 6. Table 6 shows that the calculated formation energy of the $O(1')_{vac}$ vacancy ranges between that for the vanadyl vacancy $O(1)_{vac}$ oxygen and those for the bridging oxygen vacancies $O(2)_{vac}$ and $O(2)_{vac}$. Thus, sub-surface oxygen vacancies are energetically of similar importance than those at or above the surface.

3.2.2. H, N, NH, NH_2, and NO adsorption

The calculations show that after reduction of the $V_2O_5(010)$ surface by introducing an oxygen vacancy most of the adsorbates will stabilize preferentially at the position of the missing oxygen where they will substitute the substrate atom. In the following, this will be called "substitutional adsorption".

Atomic hydrogen is found to adsorb at all surface oxygen vacancy sites $O(1)_{vac}$, $O(2^{(')})_{vac}$, $O(3^{(')})_{vac}$, where its stable position coincides almost with that of the missing oxygen before it was removed, described as substitutional adsorption. Surface binding leads to reasonably large H adsorption energies E_{ads}(H) where, according to Table 3, the bridging vacancies, $O(2^{(')})_{vac}$ and $O(3^{(')})_{vac}$, sites with E_{ads}(H) = -2.6 eV are energetically preferred over the vanadyl vacancy site $O(1)_{vac}$ with E_{ads}(H) = -1.4 eV. Interestingly, the adsorption energies, corresponding to hydrogen being bound to reduced vanadium neighbors at $O(2^{(')})_{vac}$, $O(3^{(')})_{vac}$, vacancies, differ from corresponding E_{ads}(H) values for hydrogen binding to surface oxygen at $O(2^{(')})$, $O(3^{(')})$ sites of the perfect surface by only little, 0.2 eV at most. In contrast, E_{ads}(H) for adsorption at the vanadyl oxygen vacancy $O(1)_{vac}$ is substantially smaller in absolute magnitude than the value for the perfect surface and is, overall, the smallest of all vacancy sites. This can be explained by the specific binding situation at the $O(1)_{vac}$ vacancy. As discussed in Sec. 3.2.1, the vanadium atom

below the $O(1)_{vac}$ vacancy moves from its initial position at the perfect $V_2O_5(010)$ surface into the substrate forming an additional bond with a vanadyl oxygen O(1) of the second physical layer. Obviously, this additional bond weakens the hydrogen binding ability of the vanadium atom compared to those near the other oxygen vacancies (where no additional bonds are formed) and results in the hydrogen adsorption energy $E_{ads}(H)$ being the smallest for the $O(1)_{vac}$ vacancy.

The geometric effect of hydrogen adsorption at the different oxygen vacancy sites $O(1)_{vac}$, $O(2^{(')})_{vac}$, and $O(3^{(')})_{vac}$, is quite obvious and intuitively clear. At all vacancy sites, the substitutional adsorption leads to hydrogen filling the oxygen site and recovering broken bonds with its vanadium neighbors. As a consequence, the relaxation of the neighboring vanadium and oxygen atoms due to vacancy formation is partially recovered. This is illustrated by Table 5 which compares the largest displacements of vanadium neighbors next to each oxygen vacancy before and after hydrogen adsorption. In particular, at the vanadyl vacancy $O(1)_{vac}$ where the vanadium shifts by 0.98 Å inwards compared with the perfect surface the shift is reduced to only 0.28 Å after hydrogen adsorption. The hydrogen adsorbate substituting missing oxygen in the vacancies is also reflected in the electronic properties. In contrast to adsorption at the perfect surface, where hydrogen becomes positively charged (q(H) = 0.6 au, as discussed in Sec. 3.1.1), adsorption at oxygen vacancy sites of the reduced surface yields a negatively charged adsorbate, q(H) at = -0.5 au. This results in vanadium neighbors which are charged more positively recovering their vacancy-induced chemical reduction to some extent.

The sub-surface vanadyl oxygen vacancy O(1') is not immediately available for substitutional adsorption. However, this vacancy can facilitate hydrogen adsorption at the surface vanadium site above it, denoted as $V/O(1')_{vac}$. The vacancy causes the vanadium to move further out of the surface (by about 0.2 Å) becoming reduced and hence more reactive. As a consequence, hydrogen which does not stabilize at the vanadium site of the perfect surface is found to adsorb at the $V/O(1')_{vac}$ site with an adsorption energy $E_{ads}(H)$ = -2.1 eV. This lies between the energy for the vanadyl $O(1)_{vac}$ and those for the bridging $O(2^{(')})_{vac}$ and $O(3^{(')})_{vac}$ sites at the reduced $V_2O_5(010)$ surface. Therefore, hydrogen adsorption at $V/O(1')_{vac}$ sites involving sub-surface oxygen vacancies must be taken into account in a complete characterization of hydrogen interacting with reduced vanadium oxide.

The calculations show that **atomic nitrogen**, as well as **NH**, **NH_2** and **NO** molecules all adsorb substitutionally at oxygen vacancy sites of the reduced V_2O_5(010) surface where the nitrogen center stabilizes always in the position of the missing oxygen, as sketched in Fig. 5. Further, atomic nitrogen and the corresponding molecules are found to adsorb at all oxygen vacancy sites with sizeable adsorption energies E_{ads} listed in Table 3 where the bridging oxygen $O(2)_{vac}$ vacancy site is always energetically preferred. The surface relaxation near the $O(1)_{vac}$, $O(2)_{vac}$, and $O(3)_{vac}$ vacancy sites induced by adsorption of these species proceeds analogous to that discussed for hydrogen. At these sites the adsorbates cause the neighboring vanadium atoms to partially recover their positions obtained for the perfect surface as quantified in Table 5 by the displacements of vanadium neighbors next to each oxygen vacancy before and after adsorption.

At the $O(2')_{vac}$ and $O(3')_{vac}$ vacancy sites located both near two vanadyl groups VO(1), see Fig. 1, adsorption of the molecules NH, NH_2 and NO causes the vanadyl groups to relax by tilting away from the corresponding vacancy sites making room to accommodate the adsorbates. This is similar to the effect discussed in Sec. 3.1.1 for hydrogen adsorption at the bridging O(2') and O(3') oxygen sites, see also Fig. 4. At the $V/O(1')_{vac}$ site of the reduced V_2O_5(010) surface atomic nitrogen as well as the above molecules can stabilize with sizeable adsorption energies E_{ads} as shown in Table 3 whereas N, NO, and NH do not bind at vanadium sites of the perfect surface and NH_2 binds only very weakly. This explained, as for hydrogen adsorption, by the reduction of the surface vanadium becoming more reactive in the presence of the sub-surface oxygen vacancy $O(1')_{vac}$. The atom relaxation due to adsorption of atomic nitrogen and of the above molecules is completely analogous to what has been found for hydrogen adsorption. The surface vanadium, which is already shifted out of the surface due to the sub-surface vacancy $O(1')_{vac}$ (by about 0.2 Å), is moved further out by about 0.5 Å as a result of binding with the adsorbate, see also Table 5.

3.2.3. NH_3 and NH_4 adsorption

Ammonia, NH_3, is found to adsorb at the reduced V_2O_5(010) surface only at vanadium sites below the vanadyl oxygen vacancy $O(1)_{vac}$ or above the sub-surface vacancy $O(1')_{vac}$, or at the

bridging vacancy site $O(3')_{vac}$. Amongst these, the $V/O(1')_{vac}$ site is energetically preferred with an adsorption energy of $E_{ads}(NH_3)$ = -1.24 eV. In contrast, NH_3 does not stabilize near the $O(2')_{vac}$ vacancy site. Further, ammonia approaching the two vacancy sites $O(2)_{vac}$ and $O(3)_{vac}$ leads to equilibration in a geometry corresponding to the $V/O(1')_{vac}$ geometry. Here the adsorption process leads to surface relaxation which is accompanied by diffusion of oxygen from the sub-surface O(1') site filling either the $O(2)_{vac}$ or $O(3)_{vac}$ vacancy. For the $O(2)_{vac}$ vacancy at the $V_2O_5(010)$ surface this diffusion is suggested already without adsorbates since the energy barrier for an optimized diffusion path at the clean surface is found to be quite low, 0.08 eV from the present cluster models. Diffusion processes as elementary steps of the catalytic NO_x Reduction with NH_3 will be discussed elsewhere[36, 62].

The computed adsorption energies for ammonia at the $O(1)_{vac}$ and $V/O(1')_{vac}$, sites of the reduced $V_2O_5(010)$ surface, $E_{ads}(NH_3)$ = -0.87 and -1.24 eV, respectively, are significantly larger than for the perfect surface where ammonia binds only weakly at the V metal site, see Table 1. Thus, surface reduction supports ammonia adsorption and can confirm the experimental observation of NH_3 adsorbates at vanadium oxide[52, 54] in contrast to the theoretical results for the perfect surface.

The **ammonium** species, NH_4, is too large to fit into any of the oxygen vacancies at the $V_2O_5(010)$ surface which excludes substitutional adsorption. As a result, the ammonium adsorbate binds to the reduced oxide surface near oxygen vacancies in a very similar way as to the perfect surface. The size of the tetrahedrally shaped NH_4 leads to equilibrium geometries which involve more than one oxygen site at the surface. This is obvious in Fig. 5 which sketches the adsorbate geometry for the energetically most favorable site near $O(3')_{vac}$ with $E_{ads}(NH_4)$ = -3.67 eV. Here NH_4 binds with its nitrogen near the center of four O(1) vanadyl oxygen groups of the surface, analogous to the result for the perfect surface, see Fig. 3. The calculations show further that the NH_4 species can stabilize near all other oxygen vacancy sites of the reduced surface with reasonably large adsorption energies E_{ads} ranging between -2.83 and -3.47 eV. Analogous to the results for the perfect surface, adsorption is mainly determined by electrostatic binding of the NH_4 species which becomes positively charged (Bader charges of about 0.8 au) and interacts with its negative image charge in the substrate. This explains the result that

adsorption energies for the ammonium species, which do not vary greatly between the different surface sites, are also rather similar and only slightly smaller for the reduced compared with the perfect V_2O_5(010) surface. In addition, these results are compatible with the experimental observation of a very stable surface NH_4^+ species[52, 54].

3.3. Vibrational properties of NH_3 and NH_4 at the V_2O_5(010) surface

The present theoretical results for surface binding of ammonia and the ammonium species at the perfect and reduced V_2O_5(010) surface can be substantiated further by examining vibrational properties of the adsorbates. These have been measured by infrared (IR) spectroscopy[52, 54] and can, thus, be used for comparison in order to test the theoretical findings. The experimental assignment of NH_x surface species is usually based on published data[74] of the fundamental IR bands of ammonia, amine groups, and ammonium ions. Here NH_3 and NH_4^+ species are identified by their symmetric and asymmetric N-H bending modes δ_s and δ_{as}. Among these the symmetric bending mode δ_s of NH_3 at 950 cm^{-1} (Ref.[74]), the so called "umbrella mode", where the nitrogen atom oscillates normal to the plane formed by the three hydrogen atoms, is of special interest. If NH_3 binds with its nitrogen end to the substrate surface, the electronic coupling is expected to cause a shift in the vibrational frequency of the umbrella mode towards higher energies. Therefore, an experimental observation of this mode can be used not only to identify adsorbed NH_3 species but a corresponding frequency shift can indicate the strength of surface binding.

Table 7 compares theoretical frequencies of vibrational δ_s, δ_{as} modes, obtained for both gas phase and adsorbed NH_x species using the present cluster models, with corresponding experimental values from IR measurements[52, 54]. In the experiments, the δ_s umbrella mode of adsorbed NH_3 is found to be shifted by 300 cm^{-1} to higher energies compared with that of the molecule in gas phase. This is confirmed qualitatively by the present calculations. However, the theoretical shift of 45 cm^{-1} for the NH_3 adsorbate at the perfect V_2O_5(010) surface, see Table 7, is much smaller than found in experiment. This is explained by the weak electronic binding at the energetically favored vanadium site of the perfect surface obtained by the present theory which

disagrees with experiments evidencing stronger chemisorptive binding of NH_3. The discrepancy has also been reported in other theoretical studies[18-20, 27, 31, 34] which failed to reproduce strong chemisorptive binding at the perfect vanadium oxide surface connected with a large frequency shift of the NH_3 umbrella mode identified in experiment[52, 54].

The present study considers, in addition, ammonia adsorption near oxygen vacancies of the reduced V_2O_5(010) surface which yields reasonably strong chemisorption as discussed in Sec. 3.2.3. This leads to a frequency shift of the δ_s umbrella mode of adsorbed NH_3 which is increased from 45 to 165 $cm^{-1}$for corresponding vanadyl oxygen vacancy sites, see Table 7. The increased shift is still too small to reproduce the experimental findings quantitatively but can provide a better interpretation. It may suggests that chemisorbed ammonia species near oxygen vacancies at the oxide surface exists in the experiment which can explain the observed vibrational frequency shifts of the δ_s umbrella mode of chemisorbed NH_3. Still better quantitative agreement between theory and experiment might be obtained by structural models of increased complexity involving surface reconstruction due to multiple oxygen vacancies. However, the present results for NH_3 adsorption at the reduced oxide surface, which has been ignored in the previous theoretical studies[18-20, 27, 31, 34], point into the right direction.

Table 7 includes also theoretical frequencies of vibrational δ_s, δ_{as} modes computed for both gas phase NH_4 and adsorbed species at the V_2O_5(010) surface as well as experimental values from IR measurements[52, 54]. The experimental frequencies of these modes are affected only little by the chemisorptive interaction resulting in shifts below 30 cm^{-1}. This is consistent with the theoretical data which yield for frequencies of δ_s modes only minor decreases due to adsorption, below 45 cm^{-1}, and for those of δ_{as} modes variations between -60 and 115 cm^{-1}. The quantitative differences compared with measured shifts are, to some extent, due to the fact that experimental gas phase values for NH_4 usually refer to ammonium attached to other molecules in gas phase[74] whereas the present theoretical data are obtained for a fictitious free NH_4^+ ion in vacuum.

4. Conclusion

The present cluster models give a clear picture of geometric, energetic, and electronic properties of the different adsorbate species that can occur at the V_2O_5(010) surface when the selective catalytic reduction (SCR) of NO in the presence of ammonia proceeds at the oxide substrate. Here one can expect as adsorbates atomic hydrogen, nitrogen, and oxygen, as well as molecular NO, NH, NH_2, NH_3, and NH_4 species. In addition, oxygen from the substrate surface and surface OH groups resulting from hydrogenation will get involved in elementary reaction steps. All surface species have been examined in the present cluster studies where local adsorption sections at the vanadium oxide surface are modeled by sufficiently large clusters with their electronic structure described by DFT methods. In addition to clusters simulating the perfect V_2O_5(010) surface we consider also clusters of the reduced surface where reduction is simulated locally by corresponding surface oxygen vacancies.

Atomic hydrogen and nitrogen are found to stabilize to all oxygen sites of the V_2O_5(010) surface but not above bare vanadium sites. At the oxygen sites the two atoms bind fairly strongly forming local surface OH and NO groups with adsorption energies E_{ads} ranging between -2.4 eV and -2.8 eV for hydrogen and between -0.5 eV and -1.5 eV for nitrogen. The inter-nuclear distances *d*(O-H) and *d*(O-N) in the adsorbed state are quite similar to values found for free OH radicals and gas phase NO. As a consequence of the adsorption, binding of the corresponding substrate oxygen with its vanadium neighbors is weakened noticeably such that diffusion and desorption of OH / NO species becomes possible. The adsorption of atomic oxygen at the V_2O_5(010) surface has been studied previously[2] and yields qualitatively similar results that those for H and N adsorption. Here the oxygen adsorbate combines with substrate oxygen to form surface peroxo O_2 groups which are weakly bound to the substrate and can easily desorb leaving oxygen vacancies behind.

Adsorbed NH and NH_2 species, resulting from NH_3 dehydrogenation at the surface, are also bound most strongly to oxygen sites at the V_2O_5(010) surface where surface binding is somewhat stronger for NH (E_{ads} between -0.8 eV and -1.0 eV) than for NH_2 (E_{ads} between -0.5 eV and -0.7 eV at O(1), O(2) sites). These radicals are too large to fit between the surface vanadyl groups near the O(2') and O(3') sites which explains why they do not stabilize at these sites. This applies also to the NO molecules which, altogether, binds only very weakly with the surface (E_{ads}

between -0.2 eV and -0.3 eV). Ammonia is found to stabilize only above vanadium sites of the perfect V_2O_5(010) surface where it binds very weakly with E_{ads} = -0.2 eV .This is in agreement with previous theoretical studies[18-22, 24, 35] but disagrees with the experimental data suggesting strong adsorption at the vanadium oxide surface[52-54]. This will be addressed in more detail below.

In contrast to NH_3, the ammonium species, NH_4, is adsorbed near all oxygen and vanadium sites of the surface except for the O(2') site where it does not fit between the adjacent surface vanadyl groups, see Figs. 1, 2a. The adsorbed ammonium binds quite strongly to the surface with E_{ads} ranging between -3.2 eV and -3.9 eV which is explained by the type of adsorptive interaction. At the surface, the ammonium species becomes positively charged and can be viewed as an NH_4^+ ion interacting with its negative image charge in the substrate which reflects an adsorption bond which is dominated by electrostatic contributions in qualitative agreement with previous theoretical studies[18-20, 27, 31, 34]. The most stable adsorbate position is found to be above four O(1) vanadyl oxygen groups where NH_4 stabilizes with three of its hydrogen atoms pointing towards the substrate and one sticking out. Other geometric arrangements published earlier[18, 19, 27, 31, 34] are identified as energetic saddle points and are explained by limited surface relaxation in the previous calculations as well as by the use of surface clusters which are too small[19, 27].

While NH_4 is very unlikely to adsorb at vanadium oxide from gas phase it can be formed as a result of ammonia binding to an OH group (Brønsted site) at the surface. Corresponding adsorption energies E_{ads}, computed for the present cluster models, range between -0.9 eV and -1.4 eV and are, thus, much larger in absolute magnitude compared with values for NH_3 binding to the perfect oxide surface. Therefore, pre-adsorbed surface OH groups can favor ammonia adsorption and may provide an explanation for the seemingly strong adsorption of ammonia at the perfect V_2O_5(010) surface observed in experiment[52-54].

Adsorption of the reactants participating in the SCR process is also studied theoretically for the reduced V_2O_5(010) substrate and shows substantial differences compared with adsorption at the perfect surface. Here chemical reduction is modeled locally by introducing surface oxygen vacancies at the perfect surface which is electronically saturated. (It should be mentioned in passing that surface reduction can also occur at vanadium pentoxide surfaces which are

terminated along directions other than (010) and result in electronically unsaturated local regions considered previously[35, 75].) Overall, most of the reactants, hydrogen, nitrogen, NO, NH, and NH_2, bind quite strongly near all surface oxygen vacancy sites of the V_2O_5(010) substrate where they stabilize in positions formerly occupied by the oxygen. This substitutional adsorption geometry results in local surface relaxation where, due to binding with the adsorbate, the vanadium and oxygen atoms near the oxygen vacancy move towards their initial positions at the surface before the vacancy was created.

In this work we consider also chemical reduction of the vanadium oxide due to sub-surface oxygen vacancies, in particular, the sub-surface vanadyl oxygen vacancy O(1') below a vanadium atom at the V_2O_5(010) surface. This vacancy can be created by oxygen diffusing from the O(1') site of the V_2O_5 bulk to the surface filling a surface oxygen vacancy. While the O(1') vacancy itself cannot act as an adsorption site, it enhances the reactivity of the surface vanadium above leading to a V/O(1')$_{vac}$ adsorption site. At this surface site, all adsorbates can bind quite strongly with adsorption energies E_{ads} between -1.2 eV to -3.6 eV which is quite different to the vanadium sites at the perfect V_2O_5(010) surface where, except for NH_4, no or only very weak (NH_2, NH_3) adsorption was found in the calculations. It suggests that sub-surface oxygen vacancies may become important for the chemical reduction of the vanadium oxide surface and, thus, may affect chemical behavior connected with the SCR process.

Ammonia, for which the calculations show only weak adsorption at the perfect V_2O_5(010) surface binds quite strongly at the O(1)$_{vac}$ and V/O(1')$_{vac}$ sites of the reduced surface (E_{ads} of -0.9 eV and -1.2 eV, respectively). Approaching NH_3 to the bridging O(2)$_{vac}$ and O(3)$_{vac}$ vacancy sites leads to the adsorbate stabilizing also in a geometry corresponding to the V/O(1')$_{vac}$ geometry. This is achieved by oxygen diffusing simultaneously from the sub-surface O(1') site to the corresponding surface oxygen vacancy which substantiates the importance of sub-surface oxygen for the NH_3 adsorption. Altogether, surface reduction is found to support ammonia adsorption at vanadium sites of the oxide surface and may suggest that the strong NH_3 adsorption observed in experiment[52, 54] involves surface defects such as oxygen vacancies. This is also confirmed by the theoretical analysis of vibrational properties of the NH_3 adsorbate in comparison with experimental IR data[52, 54].

Ammonium resulting from ammonia hydrogenation at the V_2O_5(010) surface or from NH_3 adsorption at surface OH Brønsted sites is found to stabilize near all oxygen surface vacancies and at the V/O(1')$_{vac}$ site. The NH_4 species is too large to fit into the vacancies which rules out substitutional adsorption. Instead, the adsorbate equilibrates near the vacancies affecting their geometry only little and leading to dominantly electrostatic binding with the substrate. This is very similar to the situation found for the perfect V_2O_5(010) surface with adsorption energies E_{ads} only slightly smaller in absolute magnitude at the reduced surface. Thus surface reduction seems to affect the behavior of the NH_4 adsorbate species much less than found for the other adsorbates which can be explained by the different type of surface bond formation of NH_4.

The present theoretical study gives a consistent account of adsorption properties of the reactants participating in the SCR process at the vanadium oxide substrate. For a full simulation of the SCR, adsorption needs to be accompanied by diffusion of the reactants at the surface as well as by hydrogenation / dehydrogenation reactions which will be discussed separately[36, 62]. These results can then serve as a basis to describe model reaction paths leading to a more detailed understanding of the SCR process on a microscopic scale.

5. Acknowledgements

M. G. is grateful for continued support by the International Max-Planck Research School (IMPRS) "Complex Surfaces in Materials Science" in Berlin. Financial support by the German Research Foundation (DFG) via its Joint Collaborative Research Center, Sfb 548 "Structure, Dynamics, and Reactivity of Transition Metal Oxide Aggregates", is greatly acknowledged.

References

[1] V.E. Henrich and P.A. Cox, *The Surface Science of Metal Oxides*, Cambridge University Press, Cambridge, 1994.

[2] K. Hermann and M. Witko, in *The Chemical Physics of Solid Surfaces*, edited by D. P. Woodruff (Elsevier, 2001), pp. 136.

[3] B. Grzybowska-Swierkosz, F. Trifiro, and J. C. Vedrine (eds.), Appl. Catal. A **157**, 1 (1997).

[4] S. F. Håkonsen and A. Holmen, in *Handbook of Heterogeneous Catalysis*, ed. by G. Ertl, H. Knötzinger, F. Schüth, J. Weitkamp (Wiley-VCH, Weinheim, 2008).

[5] F. Näumann and M. Schulz, in *Handbook of Heterogeneous Catalysis*, ed. by G. Ertl, H. Knötzinger, F. Schüth, J. Weitkamp (Wiley-VCH, Weinheim, 2008).

[6] R. K. Grasselli and M. A. Tenhover, in *Handbook of Heterogeneous Catalysis*, ed. by G. Ertl, H. Knötzinger, F. Schüth, J. Weitkamp (Wiley-VCH, Weinheim, 2008).

[7] R. K. Grasselli, J. D. Burrington, D. J. Buttrey, P. DeSanto, C. G. Lugmair, A. F. Volpe, and T. Weingand, Top. Catal. **23**, 5 (2003).

[8] P. Gabrielsson and H. G. Pedersen, in *Handbook of Heterogeneous Catalysis*, ed. by G. Ertl, H. Knötzinger, F. Schüth, J. Weitkamp (Wiley-VCH, Weinheim, 2008).

[9] G. Busca, L. Lietti, G. Ramis, and F. Berti, Appl. Catal. B: Environmental **18**, 1 (1998).

[10] L. J. Alemany, F. Berti, G. Busca, G. Ramis, D. Robba, G. P. Toledo, and M. Trombetta, Appl. Catal. B **10**, 299 (1996).

[11] H. Bosch and F. J. Janssen, Catal. Today **2**, 369 (1988).

[12] S. M. Cho, Chem. Eng. Prog. **90**, 39 (1994).

[13] P. Forzatti and L. Lietti, Heterogen. Chem. Rev. **3**, 33 (1996).

[14] F. J. J. G. Janssen, in *Handbook of Heterogeneous Catalysis*, ed. by G. Ertl, H. Knötzinger, J. Weitkamp (Wiley-VCH, Weinheim, 1997).

[15] S. C. Wood, Chem. Eng. Prog. **90**, 33 (1994).

[16] M. Farber and S. P. Harris, J. Phys. Chem. **88**, 680 (1984).

[17] F. Gilardoni, J. Weber, and A. Baiker, J. Phys. Chem. A **101**, 6069 (1997).

[18] M. Anstrom, N.-Y. Topsøe, and J. A. Dumesic, J. Catal. **213**, 115 (2003).

[19] S. Soyer, A. Uzun, S. Senkan, and I. Onal, Catal. Today **118**, 268 (2006).

[20] R.-M. Yuan, G. Fu, X. Xu, and H.-L. Wan, Phys. Chem. Chem. Phys. **13**, 453 (2011).

[21] A. Vittadini, M. Casarin, and A. Selloni, J. Phys. Chem. B **109**, 1652 (2005).

[22] E. W.-G. Diau and S. C. Smith, J. Chem. Phys. **106**, 9236 (1997).

[23] X. Duan and M. Page, J. Mol. Struct. TEOCHEM **333**, 233 (1995).

[24] P. Mars and D. W. van Krevelen, Chem. Eng. Sci. **3**, 41 (1954).

[25] F. J. J. G. Janssen, F. M. G. Van den Kerkhof, H. Bosch, and J. R. H. Ross, J. Phys. Chem. **91**, 5921 (1987).

[26] F. J. J. G. Janssen, F. M. G. Van den Kerkhof, H. Bosch, and J. R. H. Ross, J. Phys. Chem. **91**, 6633 (1987).

[27] F. Gilardoni, J. Weber, and A. Baiker, Int. J. Quant. Chem. **61**, 683 (1997).

[28] R. Družinić, Ph.D. dissertation, Freie Universität Berlin, Berlin, 1999.

[29] C. Friedrich, Ph.D. dissertation, Freie Universität Berlin, Berlin, 2004.

[30] K. Hermann, M. Witko, R. Družinić, and R. Tokarz, Appl. Phys. A **72**, 429 (2001).

[31] T. Homann, T. Bredow, and K. Jug, Surf. Sci. **515**, 205 (2002).

[32] J. Goclon, R. Grybos, M. Witko, and J. Hafner, Phys. Rev. B **79**, 075439 (2009).

[33] X. Yin, H. Han, A. Endou, M. Kubo, K. Teraishi, A. Chatterjee, and A. Miyamoto, J. Phys. Chem. B **103**, 1263 (1999).

[34] X. Yin, H. Han, I. Gunji, A. Endou, S. S. Cheettu Ammal, M. Kubo, and A. Miyamoto, J. Phys. Chem. B **103**, 4701 (1999).

[35] H. Yao, Y. Chen, Y. Wei, Z. Zhao, Z. Liu, and C. Xu, Surf. Sci. **606**, 1739 (2012).

[36] M. Gruber, Ph.D. dissertation, Freie Universität Berlin, Berlin, 2012.

[37] H. G. Bachmann, F. R. Ahmed, and W. H. Barnes, Z. Kristallogr. **115**, 110 (1961).

[38] A. Byström, K.-A. Wilhelmi, and O. Brotzen, Acta Chem. Scand. **4**, 1119 (1950).

[39] R. W. G. Wyckoff, *Crystal Structures* (Interscience, Wiley, New York, 1965).

[40] A. Chakrabarti, K. Hermann, R. Družinić, M. Witko, F. Wagner, and M. Petersen, Phys. Rev. B **59**, 10583 (1999).

[41] V. Eyert and K.-H. Höck, Phys. Rev. B **57**, 12727 (1998).

[42] X. Yin, A. Fahmi, A. Endou, R. Miura, I. Gunji, R. Yamauchi, M. Kubo, A. Chatterjee, and A. Miyamoto, Appl. Surf. Sci. **130-132**, 539 (1998).

[43] K. Hermann and L. G. M. Pettersson, deMon developers group, StoBe software V. 3.6, 2011, see http://www.fhi-berlin.mpg.de/KHsoftware/StoBe/.

[44] J. P. Perdew, K. Burke, and M. Ernzerhof, Phys. Rev. Lett. **77**, 3865 (1996).

[45] J. P. Perdew, K. Burke, and M. Ernzerhof, Phys. Rev. Lett. **78**, 1396 (1997).

[46] J. P. Perdew, K. Burke, and Y. Wang, Phys. Rev. B **54**, 16533 (1996).

[47] B. Hammer, L. B. Hansen, and J. K. Nørskov, Phys. Rev. B **59**, 7413 (1999).

[48] R. F. W. Bader, *Atoms in Molecule, A Quantum Theory* (Clarendon Press, Oxford, 1990), Vol. 22, International Series of Monographs on Chemistry.

[49] J. Sauer and J. Döbler, Dalt. Trans. 3116 (2004).

[50] D. O. Scanlon, A. Walsh, B. J. Morgan, and G. W. Watson, J. Phys. Chem. C **112**, 9903 (2008).

[51] L. Lietti and P. Forzatti, J. Catal. **147**, 241 (1994).

[52] Y. V. Belokopytov, K. M. Kholyavenko, and S. V. Gerei, J. Catal. **60**, 1 (1979).

[53] R. A. Rajadhyaksha and H. Knözinger, Appl. Catal. **51**, 81 (1989).

[54] G. Ramis, L. Yi, and G. Busca, Catal. Today **28**, 373 (1996).

[55] T. Z. Srnak, J. A. Dumesic, B. S. Clausen, E. Törnqvist, and N. Y. Topsøe, J. Catal. **135**, 246 (1992).

[56] G. T. Went, L. J. Leu, S. J. Lombardo, and A. T. Bell, J. Phys. Chem. **96**, 2235 (1992).

[57] M. Calatayud, B. Mguig, and C. Minot, Surf. Sci. Rep. **55**, 169 (2004).

[58] Q. Liu, Z. Liu, and C. Li, Chin. J. Cat. **27**, 636 (2006).

[59] G. Ramis, G. Busca, F. Bregani, and P. Forzatti, Appl. Catal. **64**, 259 (1990).

[60] H. Miyata, N. Yoshiro, O. Takehiko, and K. Yukata, Chem. Lett. **12**, 1141 (1938).

[61] M. S. Went and J. A. Reimer, J. Am. Chem. Soc. **114**, 5768 (1992).

[62] M. Gruber and K. Hermann, J Chem. Phys. (2013), to be submitted.

[63] "*Structure of free molecules in the gas phase"* in *CRC handbook of chemistry and physics*, ed. by W. M. M. Haynes (CRC Taylor and Francis, 2011), pp. 9.

[64] M. Ganduglia-Pirovano and J. Sauer, Phys. Rev. B **70**, 045422 (2004).

[65] M. V. Ganduglia-Pirovano, A. Hofmann, and J. Sauer, Surf. Sci. Rep. **62**, 219 (2007).

[66] S. Laubach, P. C. Schmidt, A. Thißen, F. J. Fernandez-Madrigal, Q.-H. Wu, W. Jaegermann, M. Klemm, and S. Horn, Phys. Chem. Chem. Phys. **9**, 2564 (2007).

[67] K. Hermann, M. Witko, and R. Družinić, Faraday Discuss. **114**, 53 (1999).

[68] K. Hermann, M. Witko, R. Družinić, and R. Tokarz, Top. Catal. **11-12**, 67 (2000).

[69] R. L. Smith, W. Lu, and G. S. Rohrer, Surf. Sci. **322**, 293 (1995).

[70] T. Oshio, Y. Sakai, and S. Ehara, J. Vac. Sci. Technol. B **12**, 2055 (1994).

[71] K. Devriendt, H. Poelman, L. Fiermans, G. Creten, and G. F. Froment, Surf. Sci. **352-354**, 750 (1996).

[72] B. Tepper, B. Richter, A. C. Dupuis, H. Kuhlenbeck, C. Hucho, P. Schilbe, M. A. bin Yarmo, and H.-J. Freund, Surf. Sci. **496**, 64 (2002).

[73] K. Hermann, M. Witko, R. Družinić, A. Chakrabarti, B. Tepper, M. Elsner, A. Gorschlüter, H. Kuhlenbeck, and H. J. Freund, J. Electr. Spectr. Rel. Phen. **98-99**, 245 (1999).

[74] A. A. Tsyganenko, D. V. Pozdnyakov, and V. N. Filimonov, J. Mol. Struct. **29**, 299 (1975).

[75] P. Hejduk, M. Witko, and K. Hermann, Top. Catal. **52**, 1105 (2009).

TABLES

Table 1

Adsorption energies, E_{ads} (in [eV]), according to (4) for H, N, NO, and NH_x, (x = 1,...,4) at different oxygen and vanadium sites of the perfect V_2O_5(010) surface represented by appropriate cluster models, see text. Table entries of "--" denote surface sites where the corresponding molecules were not found to bind.

E_{ads}	O(1)	O(2)	O(2')	O(3)	O(3')	V
H	-2.64	-2.76	-2.62	-2.52	-2.36	--
N	-1.54	-1.09	-0.53	-0.51	--	--
NO	-0.28	-0.20	--	--	--	--
NH	-0.95	-0.76	--	-0.06	--	--
NH_2	-0.46	-0.74	--	-0.16	--	-0.12
NH_3	--	--	--	--	--	-0.25
NH_4	-3.90	-3.57	--	-3.27	-3.23	-3.38
NH_3 at OH	-1.40	-0.88	--	-0.89	-1.01	--

Table 2

Characteristic inter-atomic distances, *d* (in [Å]), between oxygen near the adsorption site and corresponding adsorbate and surface vanadium centers. The data refer to H, N, NO, and NH_x, (x = 1,...,4) adsorption at different oxygen and vanadium sites of the perfect V_2O_5(010) surface represented by appropriate cluster models, see text. Atom distances *d*(V-O) at the perfect V_2O_5(010) surface (obtained from cluster calculations) are included for comparison.

		O(1)	**O(2)**	**O(2')**	**O(3)**	**O(3')**	**V**
Substrate	*d*(V-O)	1.59	1.81 1.81	1.81 1.81	1.90 1.90 2.02	1.90 1.90 2.02	--
H	*d*(O-H) *d*(V-O)	0.98 1.77	0.98 1.97 1.97	0.98 2.00 2.00	0.98 2.05 2.05 2.17	0.97 2.05 2.05 2.28	-- --
N	*d*(O-N) *d*(V-O)	1.21 1.84	1.30 2.04 2.05	1.28 2.03 2.35	1.32 2.14 2.14 2.34	-- --	-- --
NO	*d*(O-N) *d*(V-O)	2.92 1.60	3.18 1.81 1.81	-- --	-- --	-- --	-- --
NH	*d*(O-N) *d*(V-O)	1.30 1.73	1.36 1.97 1.98	-- --	1.44 2.02 2.02 2.19	-- --	-- --
NH_2	*d*(O-N) / *d*(V-N) *d*(V-O)	1.40 1.75	1.45 1.94 1.96	-- --	1.47 2.06 2.07 2.21	-- --	2.75 --
NH_3	*d*(V-N)	--	--	--	--	--	2.70
NH_4	*d*(O-NH_4) / *d*(V-NH_4) *d*(V-O)	1.81 2.28 1.63 1.61	-- --	1.79 1.85	1.56 2.08 1.95 1.95 2.05	1.64 2.15 1.96 1.96 2.07	1.81 1.82 --

Table 3

Adsorption energies, E_{ads} (in [eV]), according to (4) for H, N, NO, and NH_x, (x = 1,...,4) at different oxygen and vanadium sites of the reduced V_2O_5(010) surface, represented by appropriate cluster models of sections near oxygen vacancy sites, see text. Table entries of "--" denote surface sites where the corresponding molecules were not found to bind.

E_{ads}	$O(1)_{vac}$	$O(2)_{vac}$	$O(2')_{vac}$	$O(3)_{vac}$	$O(3')_{vac}$	$V/O(1')_{vac}$
H	-1.41	-2.59	-2.59	-2.60	-2.60	-2.08
N	-2.17	-4.10	-4.10	-3.81	-3.81	-2.72
NO	-1.00	-1.96	-1.59	-1.11	-0.87	-1.38
OH	-3.12	-4.60	-4.47	-4.11	-3.95	--
NH	-3.16	-4.92	-4.48	-4.58	-4.45	-3.58
NH_2	-2.25	-3.90	-3.35	-2.93	-3.02	-2.84
NH_3	-0.87	→ $V/O(1')_{vac}$	--	→ $V/O(1')_{vac}$	-0.31	-1.24
NH_4	-3.25	-2.83	-3.47	-3.20	-3.67	-2.84

Table 4

Characteristic inter-atomic distances, *d* (in [Å]), between surface vanadium centers adjacent to the adsorption site (oxygen vacancy) and corresponding adsorbate centers. The data refer to H, N, NO, and NH_x, (x = 1,...,4) adsorption at different oxygen vacancy sites $O(X)_{vac}$ of the reduced $V_2O_5(010)$ surface represented by appropriate cluster models, see text.

		$O(1)_{vac}$	**$O(2)_{vac}$**	**$O(2')_{vac}$**	**$O(3)_{vac}$**	**$O(3')_{vac}$**	**$V/O(1')_{vac}$**
H	*d*(V-H)	1.61	1.87 1.87	1.87 1.87	1.88 1.88 2.16	1.88 1.88 2.16	1.60
N	*d*(V-N)	1.69	1.84 1.84	1.84 1.84	1.93 1.93 2.05	1.93 1.93 2.05	1.67
NO	*d*(V-N)	1.76	2.01 2.01	2.00 2.04	2.02 2.02 2.39	2.10 2.10 2.60	1.76
NH	*d*(V-N)	1.64	1.88 1.88	1.90 1.90	1.98 1.98 2.08	1.99 1.99 2.07	1.64
NH_2	*d*(V-N)	1.83	2.06 2.06	2.07 2.07	2.10 2.10 2.54	2.09 2.09 2.96	1.83
NH_3	*d*(V-N)	2.21	--	--	--	3.54 3.54 2.58	2.10
NH_4	*d*(V-NH_4)	4.03	3.02 3.02	3.12 3.12	2.90 2.92 2.90	2.94 3.60 5.03	2.75

Table 5

Largest displacements (in [Å]) of vanadium centers adjacent to oxygen vacancies $O(1^{(,)})_{vac}$, $O(2^{(,)})_{vac}$, and $O(3^{(,)})_{vac}$, after adsorption of H, N, NO, and NH_x, (x = 1,...,4), see text. The topmost entry line "vac. cluster" denotes corresponding vanadium displacements near the vacancies before adsorption.

	$O(1)_{vac}$	$O(2)_{vac}$	$O(2')_{vac}$	$O(3)_{vac}$	$O(3')_{vac}$	$V/O(1')_{vac}$
vacancy cluster	0.98	0.43	0.43	0.05	0.05	0.20
H	0.28	0.12	0.12	0.04	0.04	0.61
N	0.06	0.18	0.18	0.07	0.07	0.83
NO	0.15	0.11	0.48	0.21	0.28	0.83
NH	0.008	0.07	0.28	0.07	0.16	0.93
NH_2	0.07	0.12	0.42	0.17	0.31	0.97
NH_3	0.79	--	--	--	0.25	0.63
NH_4	0.99	0.45	0.45	0.06	0.06	0.19

Table 6

Oxygen vacancy formation energies, $E_D(O)$, $E_D(½O_2)$ (in [eV]), according to (6), (7) for different oxygen sites at the $V_2O_5(010)$ surface, represented by appropriate cluster models of sections near oxygen vacancy sites, see text. Note that vacancy energies for $O(2)_{vac}$, $O(2')_{vac}$ and for $O(3)_{vac}$, $O(3')_{vac}$ sites are given identical numerical values which is due to symmetry constraints as explained in the text.

	$\mathbf{O(1)_{vac}}$	$\mathbf{O(2^{(,)})_{vac}}$	$\mathbf{O(3^{(,)})_{vac}}$	$\mathbf{O(1')_{vac}}$
$\boldsymbol{E_D(O)}$	4.98	6.44	6.18	5.69
$\boldsymbol{E_D(½O_2)}$	2.19	3.65	3.39	2.90

Table 7

Vibrational frequencies of δ_s, δ_{as} modes obtained for NH_3 and NH_4 species where gas phase values are compared with those for corresponding adsorbates at the V_2O_5(010). The theoretical data are calculated using the present cluster models while the experimental values refer to IR measurements, see text. All frequencies are given in [cm^{-1}] units.

	δ_s NH_3	**δ_{as} NH_3**	**δ_s NH_4**	**δ_{as} NH_4**
Theory				
gas phase	1066	1639	1703	1450
		1640	1704	1451
				1452
perfect V_2O_5,	1111	1628	1669	1350
V site		1635	1694	1439
				1510
reduced V_2O_5,	1232	1616	1659	1336
$O(1)_{vac}$ site		1649	1692	1446
				1505
reduced V_2O_5,	1226	1614	1679	1345
$V/O(1')_{vac}$ site		1619	1698	1461
				1530
Experiment				
gas phase[74]	950	1628	1680	1400
V_2O_5(010)[52]	1260	1620	--	1425
V_2O_5(010)[54]	1249	1605	1680	1425

FIGURE CAPTIONS

Fig. 1. Crystal structure of orthorhombic V_2O_5 for a view along the (001) direction (perpendicular to the (010) direction, cp. crystal axes a, b, c at the bottom). The topmost physical (010) layer is emphasized by shading. Vanadium atoms are shown by large yellow and oxygen by smaller red balls. Neighboring atom centers are connected by sticks to visualize structural properties. The non-equivalent oxygen centers, $O(1^{(,)} - 3^{(,)})$ of the crystal surface are labeled accordingly, see text. In the second physical layer the shapes of octahedral VO_6 (left) and bipyramidal V_2O_8 (right) crystal building units are outlined.

Fig. 2 Cluster models used to model different sections of the perfect and reduced $V_2O_5(010)$ surface: (a) $V_{10}O_{31}H_{12}$, (b) $V_{14}O_{46}H_{22}$, (c) $V_{14}O_{42}H_{14}$, (d) $V_{12}O_{40}H_{20}$, and (e) $V_{12}O_{40}H_{20}{}^{*}$, see text. Vanadium atoms are shown by large yellow, oxygen by smaller red, and saturating hydrogen by very small gray balls. Corresponding oxygen sites are labeled accordingly.

Fig. 3 Energetically most preferred equilibrium structures of H, N, NO, and NH_x, (x = 1,...,4) at the perfect $V_2O_5(010)$ surface, see text. Vanadium atoms are shown by large yellow balls, oxygen and nitrogen centers by smaller red and green balls, respectively, and hydrogen by very small blue balls. Surface atoms that are included in the optimization (in addition to the adsorbate) are shown as painted balls.

Fig. 4 Equilibrium geometry of hydrogen adsorbed at the O(2') site of the perfect $V_2O_5(010)$ surface. Vanadium centers are shown by large yellow balls, oxygen centers by smaller red balls, adsorbed hydrogen by very small blue balls and saturating hydrogen by small bright gray balls. Surface atom positions before adsorption are indicated by white balls.

Fig. 5 Energetically most preferred equilibrium structures of H, N, NO, and NH_x, (x = 1,...,4) at the reduced $V_2O_5(010)$ surface, see text. Vanadium atoms are shown by large yellow balls, oxygen and nitrogen centers by smaller red and green balls, respectively, and hydrogen by very small blue balls. Surface atoms that are included in the optimization

(in addition to the adsorbate) are shown as painted balls. Oxygen vacancy centers are indicated by small black dots.

Fig. 6 Sub-surface oxygen O(1') vacancy cluster $V_{12}O_{39}H_{20}^{*}$, in (a) perspective and (b) top view. Vanadium centers are shown by large yellow balls, oxygen centers by smaller red balls, and very small gray balls refer to hydrogen centers. The position of the missing oxygen atom is indicated by a small black dot. Atoms considered in the geometry optimization are labeled by a cross.

FIGURES

Fig. 1

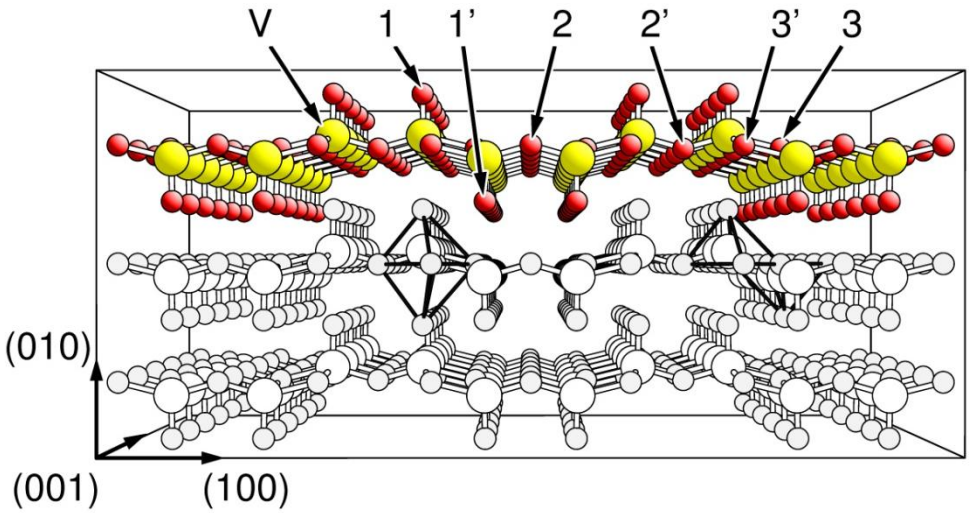

Fig. 2

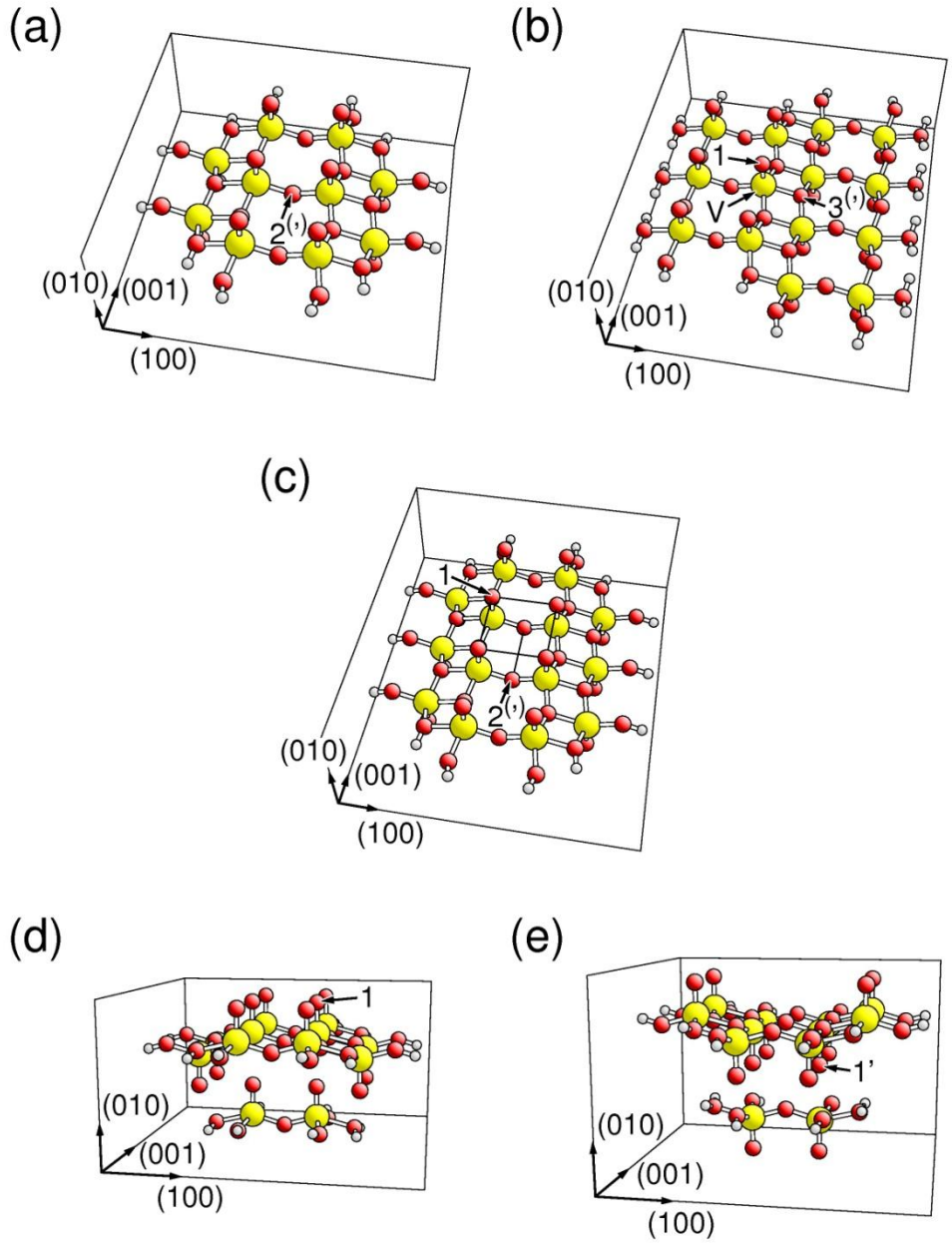
(a)
2(')
(010)
(001)
(100)
(b)
1
V
3(')
(010)
(001)
(100)
(c)
1
2(')
(010)
(001)
(100)
(d)
1
(010)
(001)
(100)
(e)
1'
(010)
(001)
(100)

Fig. 3

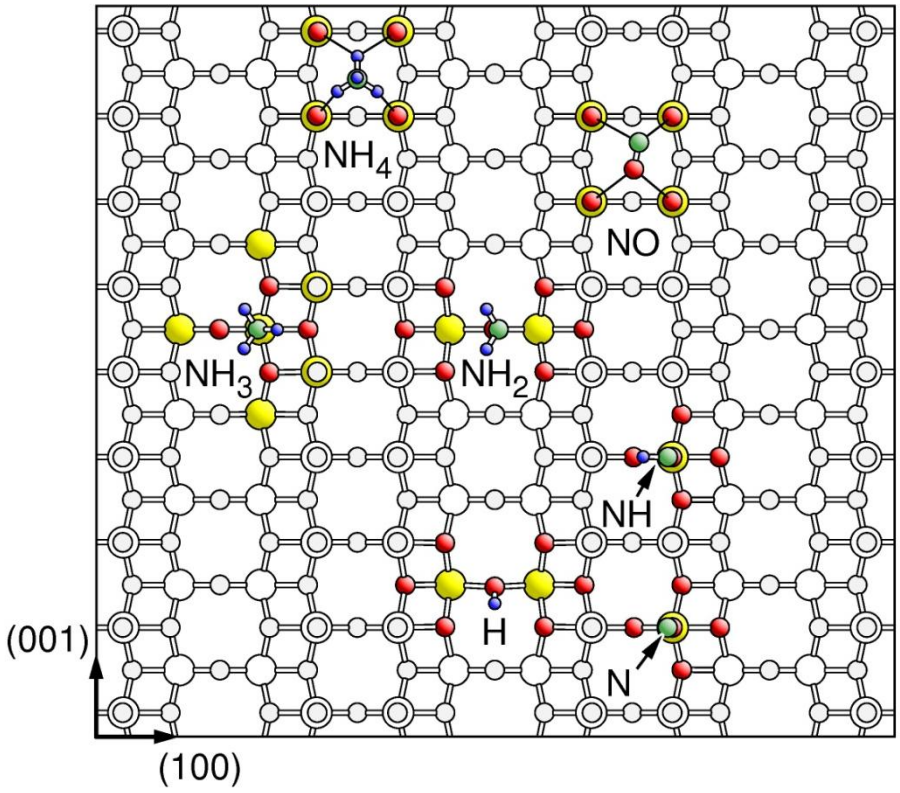

Fig. 4

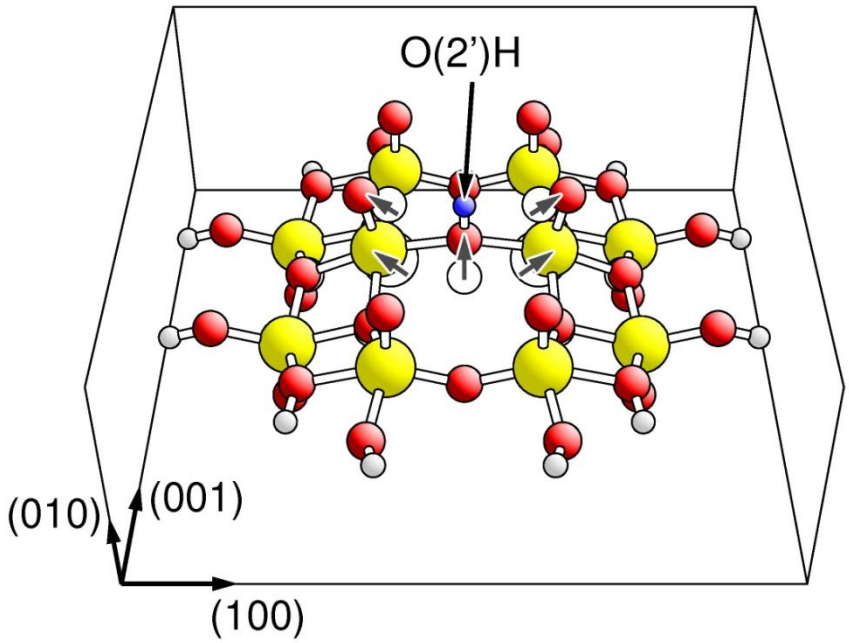

Fig. 5

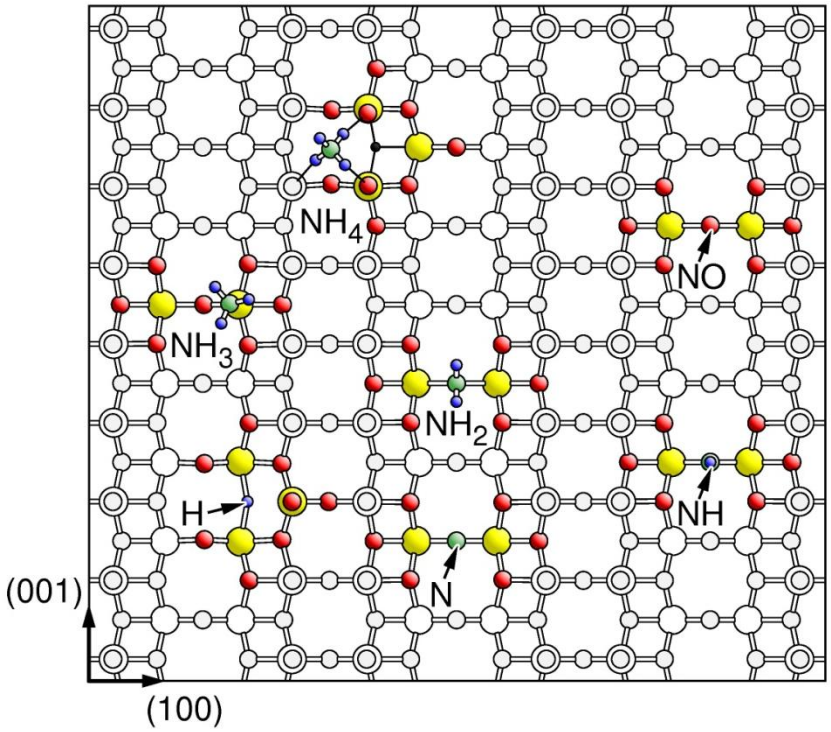

Fig. 6